Supporting Information for

Structurally Flexible 2D Spacer for Suppressing the Electron-Phonon Coupling Induced Nonradiative Decay in Perovskite Solar Cells

Ruikun Cao[1,2,#], Kexuan Sun[1,#], Chang Liu[1,*], Yuhong Mao[4], Wei Guo[1], Ping Ouyang[1], Yuanyuan Meng[1], Ruijia Tian [1], Lisha Xie[1], Xujie Lü[4], and Ziyi Ge[1,3,*]

[1] Zhejiang Provincial Engineering Research Center of Energy Optoelectronic Materials and Devices, Ningbo Institute of Materials Technology & Engineering, Chinese Academy of Sciences, Ningbo 315201, P. R. China

[2]School of Materials Science and Chemical Engineering Ningbo University, Ningbo 315211, P. R. China

[3] Center of Materials Science and Optoelectronics Engineering University of Chinese Academy of Sciences, Beijing 100049, P. R. China

[4] Center for High Pressure Science and Technology Advanced Research (HPSTAR), Shanghai 201203, P. R. China

[#]Ruikun Cao and Kexuan Sun contributed equally to this work.

*Corresponding authors. E-mail: liuchang1@nimte.ac.cn (Chang Liu); geziyi@nimte.ac.cn (Ziyi Ge)

Supplementary Figures

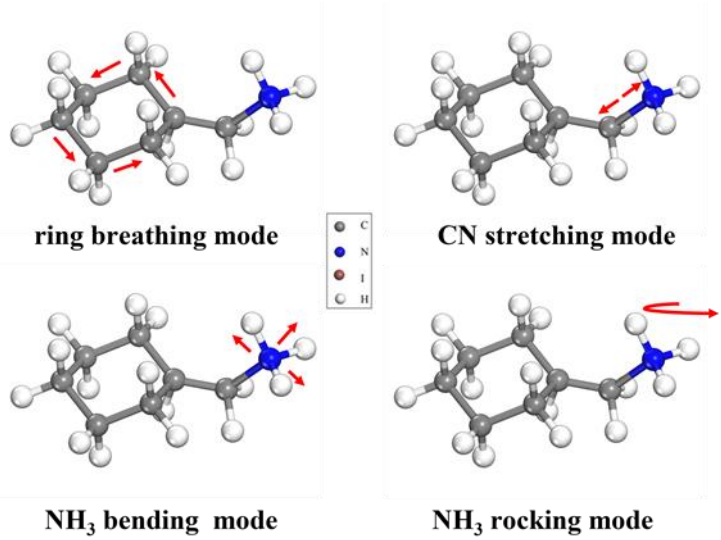

Fig. S1 Relevant vibrational modes in CMA^+

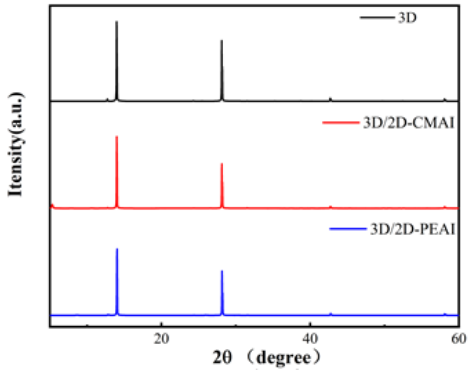

Fig. S2 X-ray diffraction patterns of 5-60° with 3D, 3D/2D-CMAI and 3D/2D-PEAI films

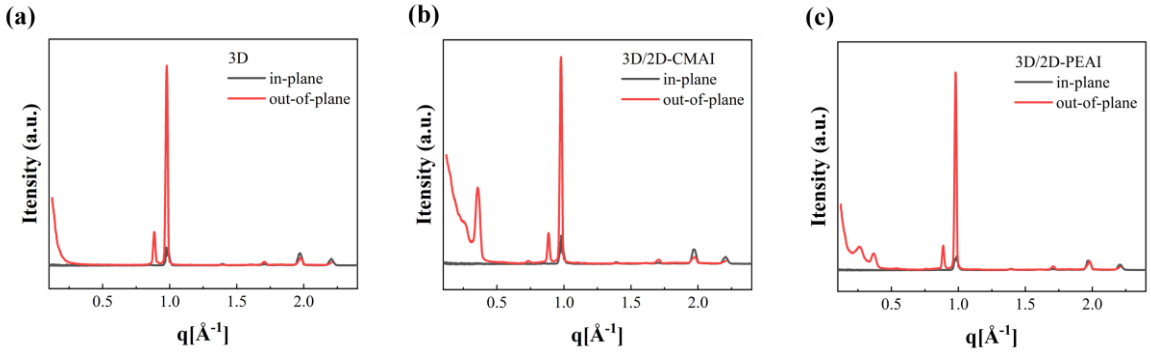

Fig. S3 The (100) in-plane and out-of-plane line cuts of GIWAX images of 3D, 3D/2D-CMAI, and 3D/2D-PEAI

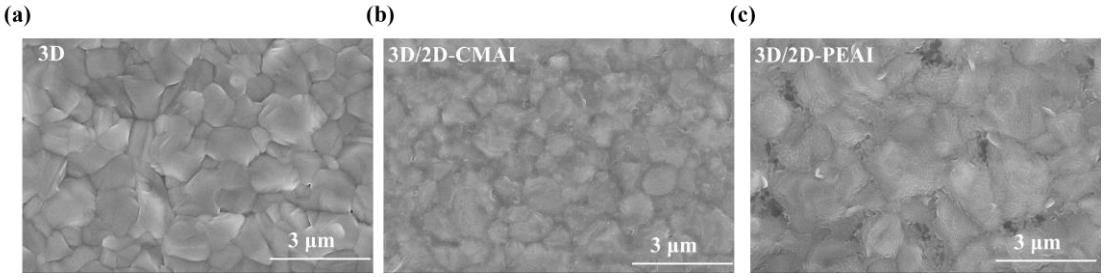

Fig. S4 SEM images of perovskite surface based on 3D, 3D/2D-CMAI, and 3D/2D-PEAI

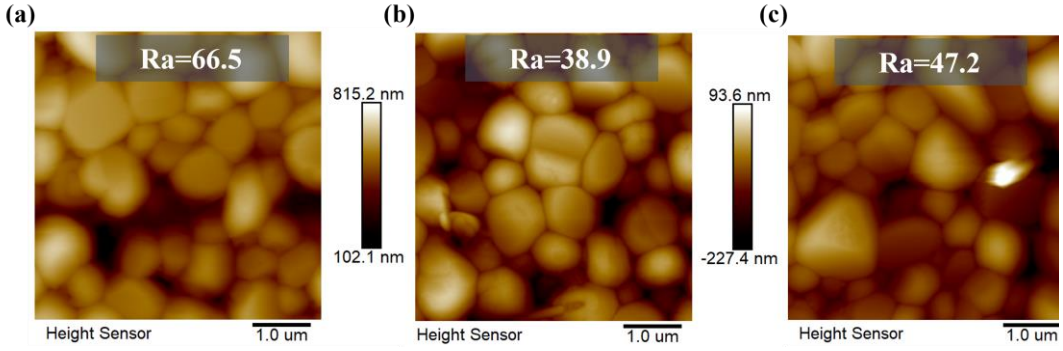

Fig. S5 AFM images of 3D, 3D/2D-CMAI, and 3D/2D-PEAI

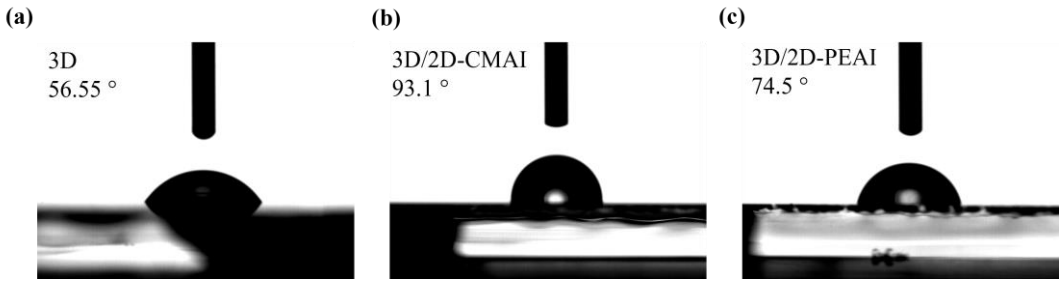

Fig. S6 Water contact angle test

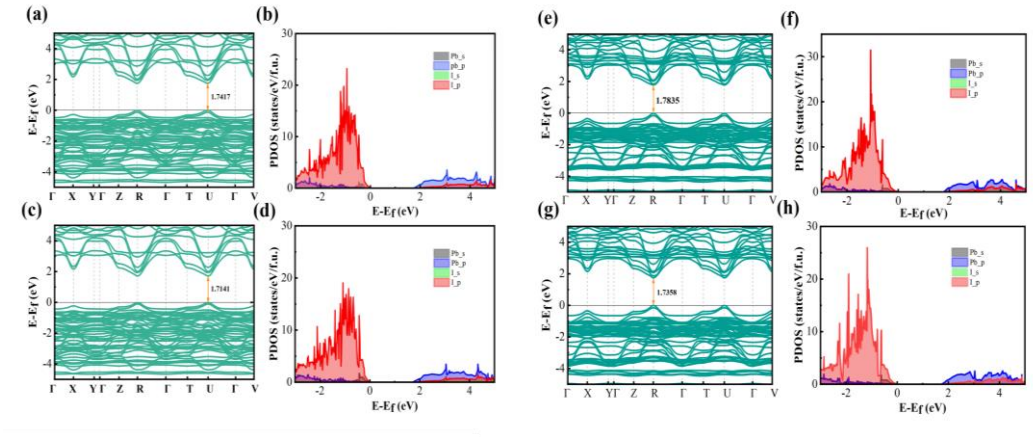

Fig. S7 a Theoretical energy band structure of $(CMA)_2FaPb_2I_7$ at 0 GPa. **b** Density of states of $(CMA)_2FaPb_2I_7$ at 0 GPa. **c** Theoretical energy band structure of $(CMA)_2FaPb_2I_7$ at 1 GPa. **d** Density of states of $(CMA)_2FaPb_2I_7$ at 1 GPa. **e** Theoretical energy band structure of $(PEA)_2FaPb_2I_7$ at 0 GPa. **f** Density of states of $(PEA)_2FaPb_2I_7$ at 0 GPa. **g** Theoretical energy band structure of $(PEA)_2FaPb_2I_7$ at 1 GPa. **h** Density of states of $(PEA)_2FaPb_2I_7$ at 1 GPa

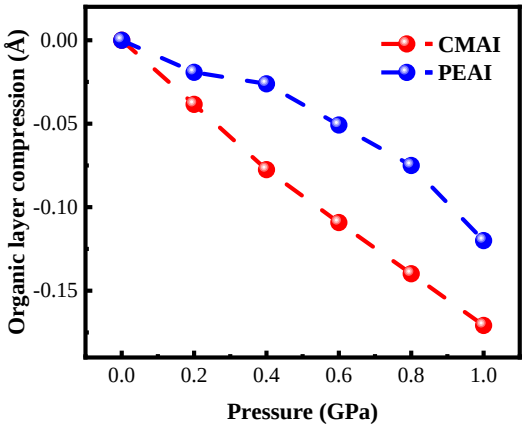

Fig. S8 Compression diagram of organic layer under 0-1Gpa

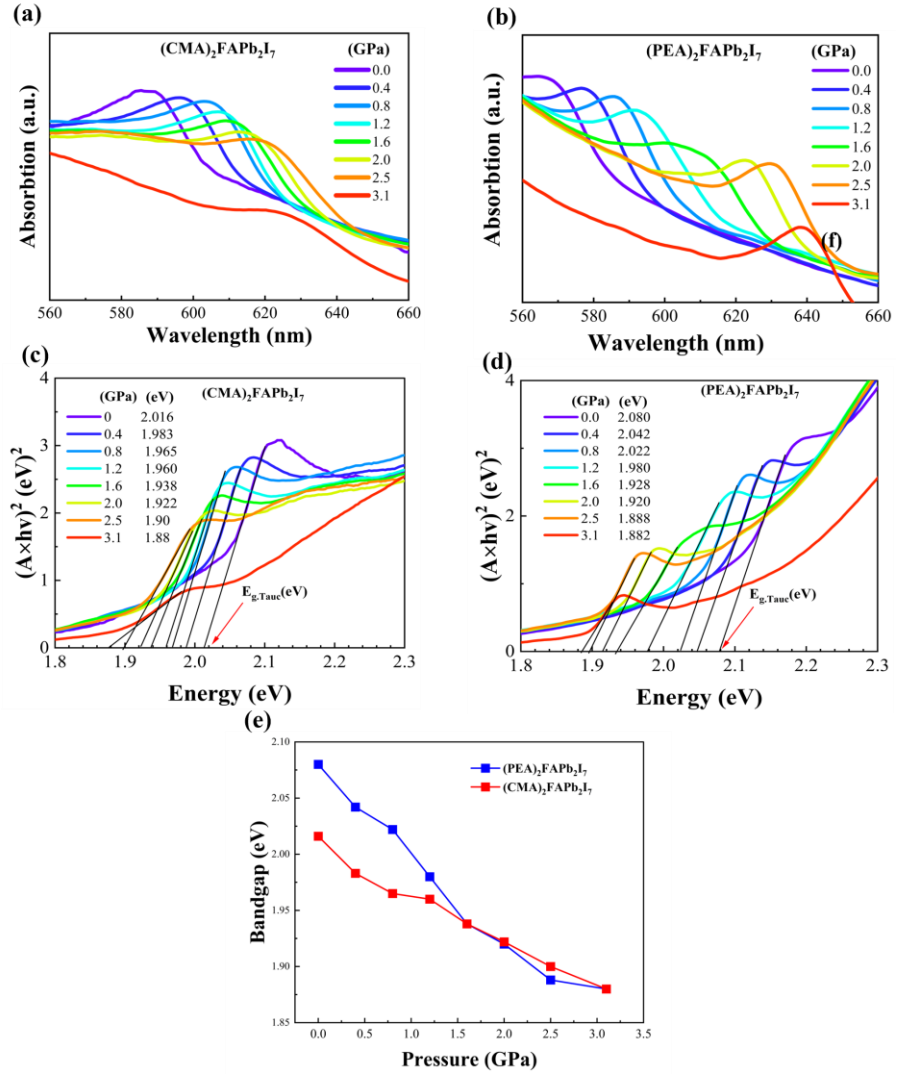

Fig. S9 a-b UV-Vis absorption spectra for the $(CMA)_2FAPb_2I_7$) and $(PEA)_2FAPb_2I_7$) target perovskite films under 0-3 GPa. **c-d** The corresponding tauc plots of UV-Vis absorption spectra. **e** Variation of the band gap of $(CMA)_2FAPb_2I_7$) and $(PEA)_2FAPb_2I_7$) with pressure change

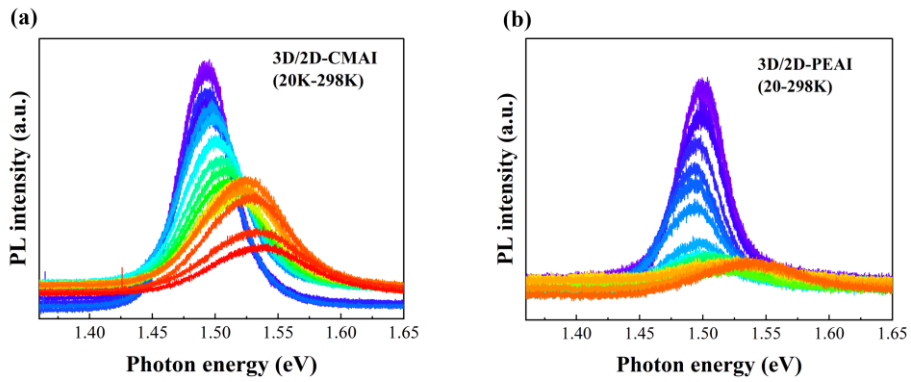

Fig. S10 a Low temperature PL testing of 3D/2D-CAMI, (b) Low temperature PL testing of 3D/2D-PEAI

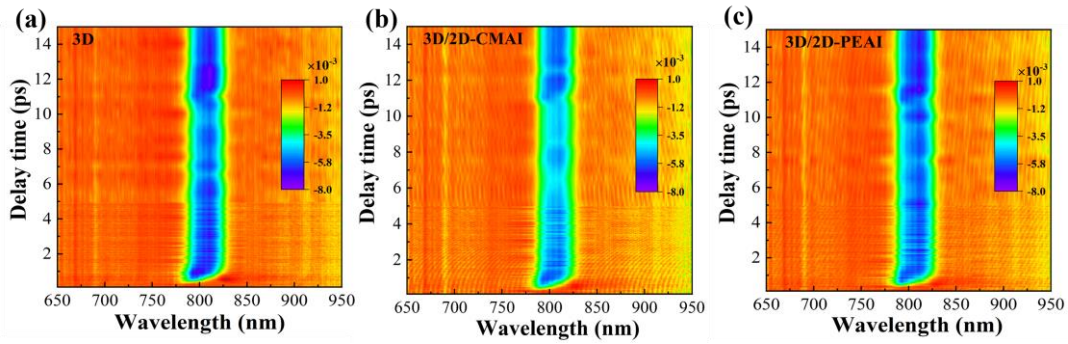

Fig. S11 Pseudocolor maps of TA spectra for 3D, 3D/2D-CMAI and 3D/2D-PEAI films

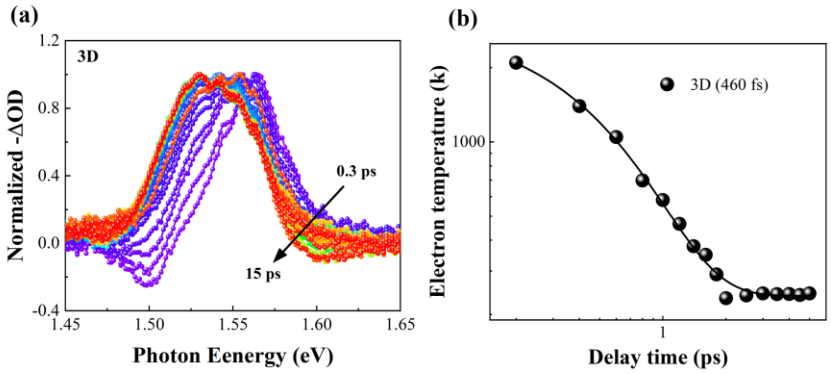

Fig. S12 a HCs at delay times from 0.3 to 15 ps for 3D. **b** Hot electron temperature decay for 3D

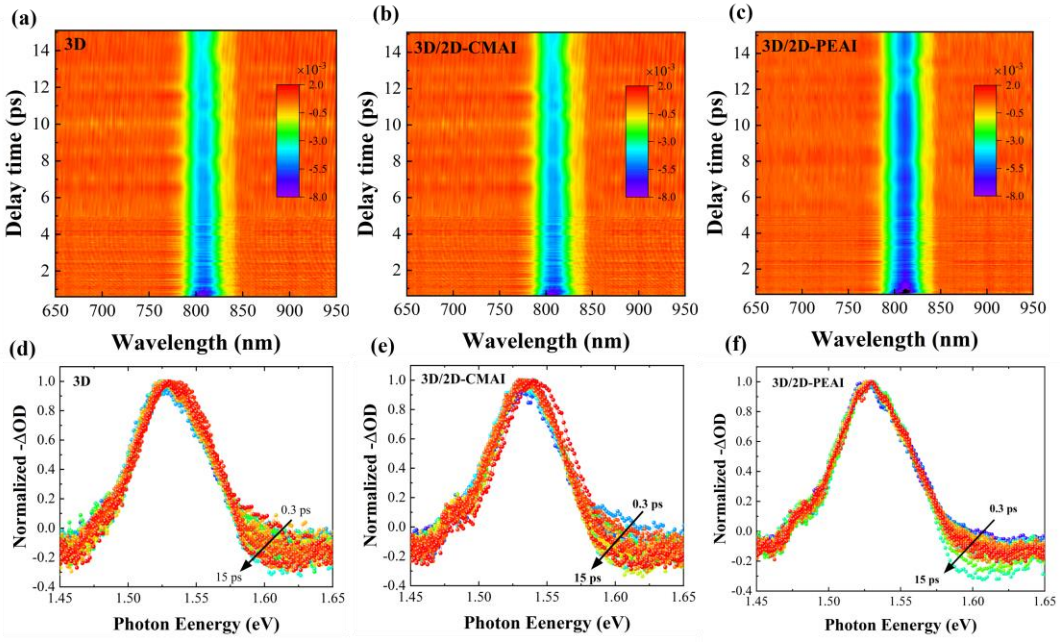

Fig. S13 Excitation at λ=800 nm **a–c** Pseudocolor maps of TA spectra for pristine 3D and 3D/2D-CMAI,3D/2D-PEAI, **d–f** HCs at delay times from 0.3 to 15 ps

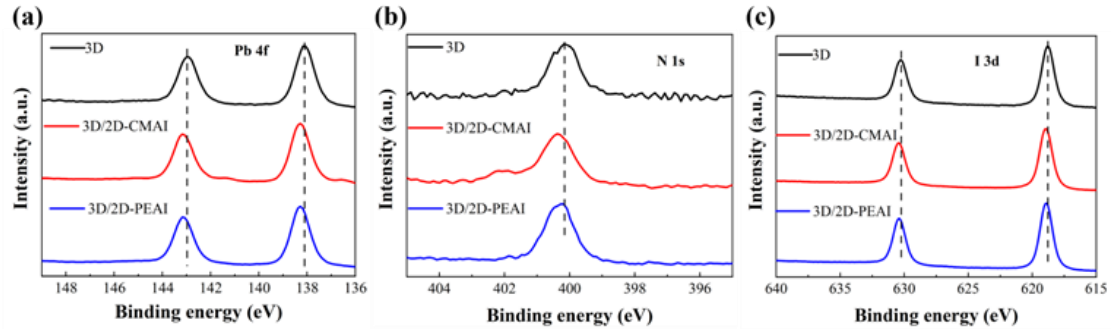

Fig. S14 High-resolution XPS spectra of Pb 4f, I 3d, and N1s

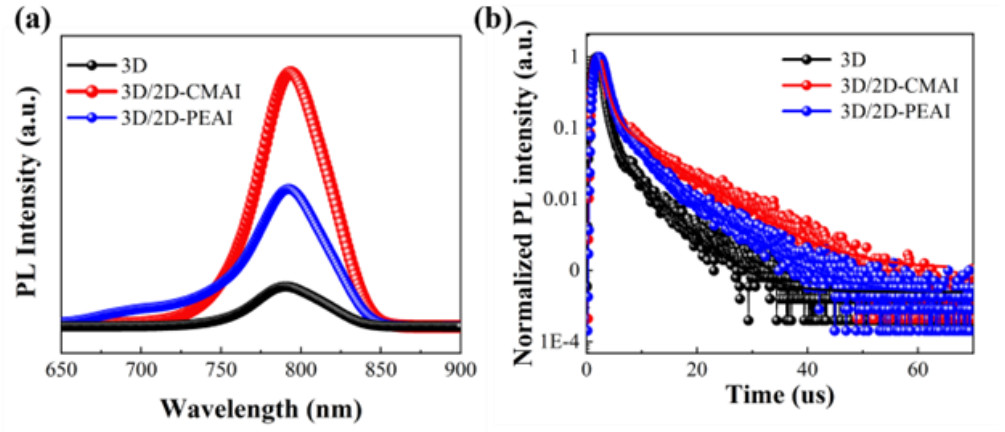

Fig. S15 Steady-state PL spectra and TRPL spectra of the pristine 3D, 3D/2D-CMAI, and 3D/2D-PEAI

Table S1 Fitting parameters for TRPL of bi-exponential decay fits

	τ_1 (μs)	τ_2 (μs)	τ (μs)
3D	0.78	5.32	0.96
3D/2D-CMAI	0.96	8.25	1.84
3D/2D-PEAI	1.17	7.11	1.74

Table S2 Summary of PSC photovoltaic efficiency based on modification of various concentrations of CMAI

CMAI	V_{OC} [a] (V)	J_{SC} [a] (mA cm^{-2})	FF [a] (%)	PCE [a] (%)
1.5 mg/ml	1.17±0.005	25.45±0.42	79.20±1.03	23.71±0.28
	(1.17)	(25.87)	(78.75)	(23.99)
3.0 mg/ml	1.18±0.006	25.53±0.59	80.71±1.16	24.43±0.40
	(1.19)	(25.46)	(81.88)	(24.83)
5mg/ml	1.19±0.01	25.74±0.26	82.11±0.97	25.23±0.29
	（1.19）	（25.73）	（83.09）	（25.52）
7 mg/ml	1.17±0.009	25.09±0.33	78.93±1.36	23.26±0.80
	(1.18)	(25.43)	(79.98)	(24.07)

[a] Average and standard deviation values were obtained based on over 10 cells from 2 different

Table S3 Summary of PSC photovoltaic efficiency based on modification of various concentrations of PEAI

PEAI	V_{OC} [a] (V)	J_{SC} [a] (mA cm^{-2})	FF [a] (%)	PCE [a] (%)
1.5 mg/ml	1.12±0.038	24.76±1.48	73.87±3.67	20.57±0.45
	(1.15)	(24.79)	(73.12)	(21.01)
3.0 mg/ml	1.14±0.014	24.57±0.40	75.59±1.78	21.36±0.43
	(1.15)	(24.47)	(77.38)	(21.79)
4.5mg/ml	1.16±0.018	24.39±0.30	77.46±0.52	22.04±0.40
	(1.16)	(24.69)	(77.98)	(22.45)
6 mg/ml	1.16±0.011	24.20±0.47	76.19±1.76	21.46±0.69
	(1.16)	(24.61)	(77.44)	(22.15)

[a] Average and standard deviation values were obtained based on over 10 cells from 2 different batches for 3D/2D-PEAI. Parameters of the best cell are reported in brackets.

Table S4 Summary of rigid PSC photovoltaic efficiency based on modification with CMAI and PEAI

Additive	V_{OC} (V)	J_{SC} (mA cm^{-2})	FF (%)	PCE (%)
3D	1.09	25.54	72.38	20.21
3D/2D-CMAI	1.19	25.73	83.09	25.52
3D/2D-PEAI	1.16	24.69	77.98	22.45

Table S5 Photovoltaic efficiency of champion PSCs based on 3D and 3D/2D-CMAI in forward and reverse scans

Additive		V_{OC}(V)	J_{SC} (mA cm^{-2})	FF (%)	PCE (%)
3D/2D-CMAI	Reverse	1.19	25.73	83.09	25.52
	Forward	1.19	25.71	82.64	25.35
3D	Reverse	1.09	25.54	72.38	20.21
	Forward	1.08	24.99	72.37	19.70

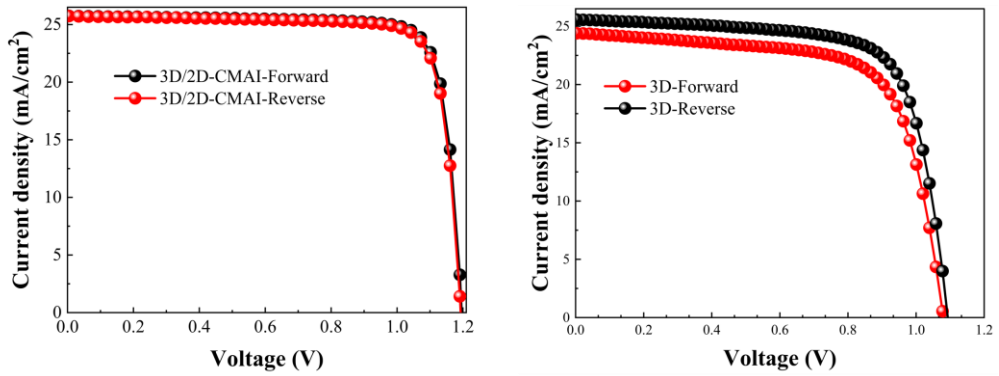

Fig. S16 J–V characteristics of optimized 3D and 3D/2D-CMAI PSCs in forward and reverse scans

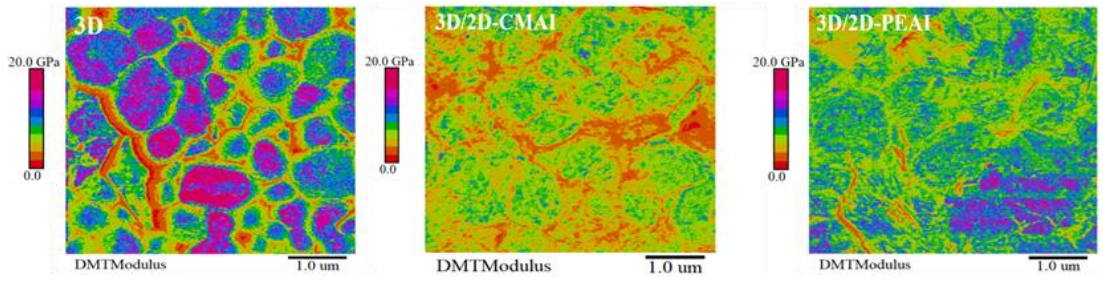

Fig. S17 DMT modulus of pristine 3D and 3D/2D-CMAI,3D/2D-PEAI

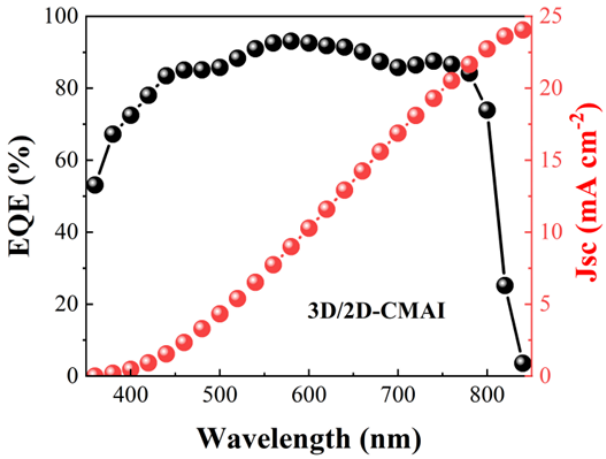

Fig. S18 The external quantum efficiency (EQE) spectra and the integrated current density of f-PSCs

Table S6 Summary of flexible PSC photovoltaic efficiency based on modification with CMAI

	V_{OC} (V)	J_{SC} (mA cm^{-2})	FF (%)	PCE (%)
3D	1.07	23.62	76.09	19.29
3D/2D-CMAI	1.20	24.87	78.39	23.41

Table S7 Summary of f-PSC photovoltaic efficiency based on 3D and 3D/2D-CMAI

	V_{OC} [a] (V)	J_{SC} [a] (mA cm^{-2})	FF [a] (%)	PCE [a] (%)
3D	1.06±0.005	22.99±0.63	74.56±1.53	18.93±0.36
	(1.17)	(23.62)	(76.09)	(19.29)
3D/2D-CMAI	1.19±0.004	24.35±0.52	77.31±1.08	23.04±0.37
	(1.20)	(24.87)	(78.39)	(23.41)

[a] Average and standard deviation values were obtained based on over 10 cells from 2 different batches for 3D and 3D/2D-CMAI. Parameters of the best cell are reported in brackets.

Table S8 The parameter of SCLC of Electron-only

Electron-only	V_{TFL} (V)	n_{trap} (cm^{-3})	μ (cm^2V^{-1} s^{-1})
3D	0.82	8.5×10^{16}	3.87×10^{-5}
3D/2D-PEAI	0.58	5.84×10^{16}	2.07×10^{-5}
3D/2D-CMAI	0.52	4.78×10^{16}	1.89×10^{-5}

Table S9 The parameter of SCLC of Hole-only

Hole-only	V_{TFL} (V)	n_{trap} (cm^{-3})	μ ($cm^2V^{-1}s^{-1}$)
3D	0.62	6.43×10^{16}	2.43×10^{-5}
3D/2D-PEAI	0.46	4.64×10^{16}	1.76×10^{-5}
3D/2D-CMAI	0.41	3.77×10^{16}	1.54×10^{-5}

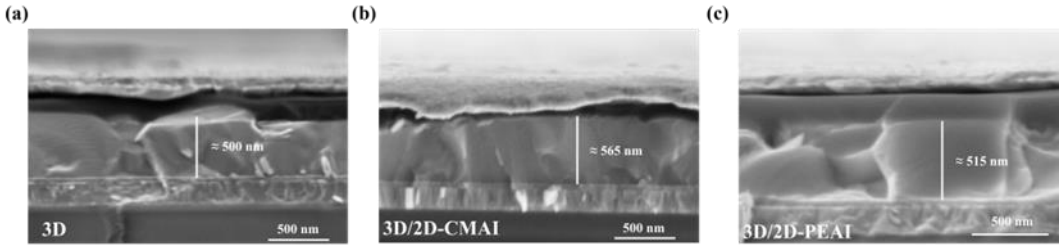

Fig. S19 SEM cross-sectional view

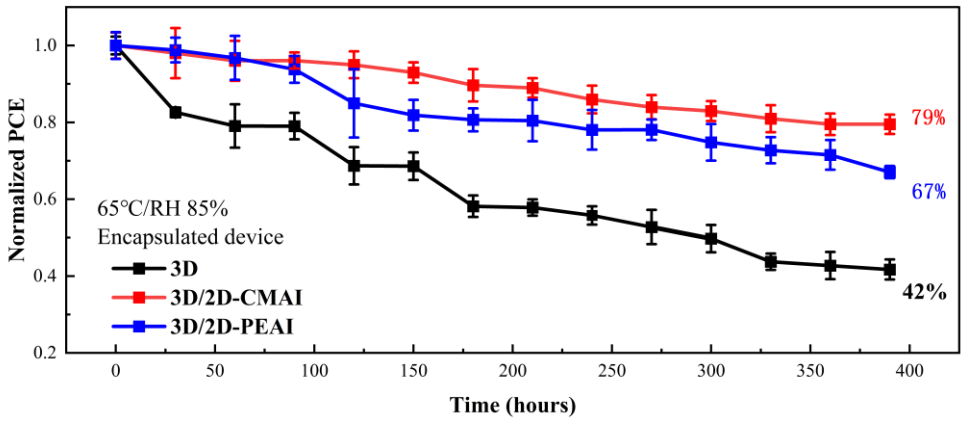

Fig. 20 ISOS-D stability test for 3D devices and 3D/2D-CMAI,3D/2D-PEAI devices